nature photonics

LETTERS

https://doi.org/10.1038/s41566-019-0428-0

Valley optomechanics in a monolayer semiconductor

Hao-Kun Li[1,4], King Yan Fong[1,4], Hanyu Zhu[1], Quanwei Li[1], Siqi Wang[1], Sui Yang[1], Yuan Wang[1,2] and Xiang Zhang[1,2,3*]

Interfacing nanomechanics with photonics and charge/spin-based electronics has transformed information technology and facilitated fundamental searches for the quantum-to-classical transition[1–3]. Utilizing the electron valley degree of freedom as an information carrier, valleytronics has recently emerged as a promising platform for developments in computation and communication[4–7]. Thus far, explorations of valleytronics have focused on optoelectronic and magnetic means[8–16]. Here, we realize valley–mechanical coupling in a resonator made of the monolayer semiconductor MoS_2 and transduce valley information into mechanical states. The coupling is achieved by exploiting the magnetic moment of valley carriers with a magnetic field gradient. We optically populate the valleys and observe the resulting mechanical actuation using laser interferometry. We are thus able to control the valley–mechanical interaction by adjusting the pump-laser light, the magnetic field gradient and temperature. Our work paves the way for realizing valley-actuated devices and hybrid valley quantum systems.

Modern electronics relies on the charge and spin to carry and store information for communication and computation. With no counterpart in free space, electrons residing in the periodic lattice of some solids possess an extra degree of freedom called the 'valley', which specifies which states the electrons occupy among the degenerate energy extrema in momentum space. By using this unique valley property to encode information, valleytronics has the potential to complement or even outperform the conventional electronics and spintronics in information processing[4–7].

To advance valleytronics, incorporating mechanical degrees of freedom is desirable. Micro-/nano-electromechanical systems (MEMS/NEMS) have revolutionized information technologies such as the internet of things[17]. Mechanical systems are intrinsically immune to electromagnetic interference and their functions as switches, filters and oscillators are ubiquitous[18]. They are also renowned for their versatility in interactions with various physical environments while maintaining low loss. Excellent mechanical sensors and transducers have been demonstrated in classical[19] and quantum[20–22] scenarios. The latter is important for studies of macroscopic quantum phenomena such as the Schrödinger cat paradox. In light of this, interfacing valleytronics with mechanics will present opportunities in fundamental studies and the application of valley physics.

With their excellent valley and mechanical properties, monolayer semiconducting transition-metal dichalcogenides are ideal candidates for exploring valley–mechanical interactions. In their electronic-band structures, the K and K′ valleys form a binary system called valley-pseudospin. A unique optical selection rule[8] arising from the strong spin–orbit coupling and the broken inversion symmetry offers a convenient way to selectively populate and manipulate the valleys with optical helicity[9–12]. Effective electrical and magnetic control of valley-pseudospin have also been demonstrated[13–16]. In addition, mechanical devices made of two-dimensional nanomaterials[23–25] exhibit high strength[26], high quality factors[27], and exceptional force and mass sensitivities[28]. The large zero-point motions resulting from the miniscule masses of such devices are desirable for the study of quantum physics.

Here we realize valley–mechanical interactions in a monolayer MoS_2 nano-resonator and directly transduce valley excitation to the mechanical states. The valley–mechanical coupling is established through a force generated from the magnetic moments of the valley-polarized carriers in the presence of a strong local magnetic field gradient. The experiment suggests a route for realizing valley-actuated devices (for example, valley transducers and valley switches) and facilitates hybridizing valley pseudospin with other information carriers (for example, microwave photons and superconducting qubits).

In transition-metal dichalcogenide monolayers, electrons at the K and K′ valleys carry opposite magnetic moments with equivalent magnitudes, resulting from the time-reversal symmetry and the broken inversion symmetry[8]. In the presence of a perpendicular magnetic field gradient, the material encounters a net force given by $F = (N_K - N_{K'})g\mu_B\nabla B$. Here, N_K and $N_{K'}$ are the carrier populations in the K and K′ valleys, g is the Lande g-factor, μ_B is the Bohr magneton and ∇B is the magnetic field gradient. The direction of the valley-mechanical force is determined by the net valley population. Through this force, the valley excitation at K (K′) can be directly transduced to the upward (downward) mechanical displacement (Fig. 1).

We fabricated the valley–mechanical device by suspending an exfoliated MoS_2 monolayer over square hole structures using the dry-transfer method (see Supplementary Information). The square holes were conformally coated with a high-permeability Ni/Fe permalloy (Fig. 2a). When a perpendicular magnetic field is applied to the sample, the permalloy structure induces a strong magnetic field gradient by distorting the local field. At the centre of the suspended MoS_2, a field gradient of about 4,000 T m^{-1} can be obtained with a magnetic field of 26 mT. The MoS_2 monolayer was characterized with photoluminescence and Raman spectroscopy (Supplementary Figs. 2 and 3). Substantial photoluminescence emission contrast between the suspended and supported zones verifies that the

[1]NSF Nanoscale Science and Engineering Center, University of California, Berkeley, CA, USA. [2]Materials Science Division, Lawrence Berkeley National Laboratory, Berkeley, CA, USA. [3]University of Hong Kong, Hong Kong, China. [4]These authors contributed equally: Hao-Kun Li, King Yan Fong.
*e-mail: xiang@berkeley.edu

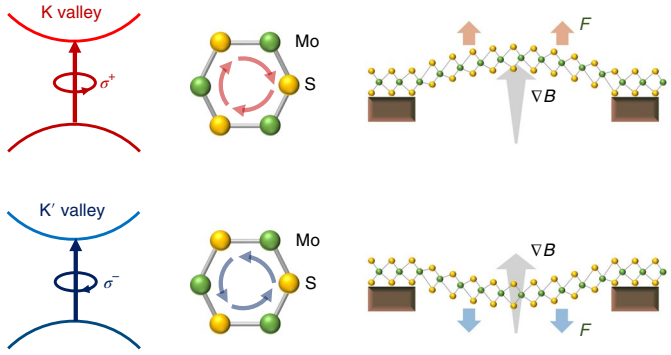

Fig. 1 | Valley-controlled mechanical motion of monolayer MoS_2. In monolayer MoS_2, the hexagonal lattice gives rise to K and K′ valleys in the band structure, which can carry information. Because of the broken inversion symmetry and strong spin–orbit coupling, K and K′ valleys can be selectively excited by circularly polarized light with helicity σ^+ and σ^-. Electrons at K and K′ valleys possess opposite Berry curvatures and undergo clockwise and anticlockwise hopping motions, which result in valley magnetic moments. Together with the magnetic moments originating from the parent atomic orbitals, the total magnetic moments carried by electrons at the two valleys are equal in magnitude while opposite in sign. In the presence of an out-of-plane magnetic field gradient ∇B, the monolayer experiences a force $F \propto (N_K - N_{K'})\nabla B$, which is proportional to the net valley population $(N_K - N_{K'})$. Therefore, a valley-controlled mechanical displacement can be attained.

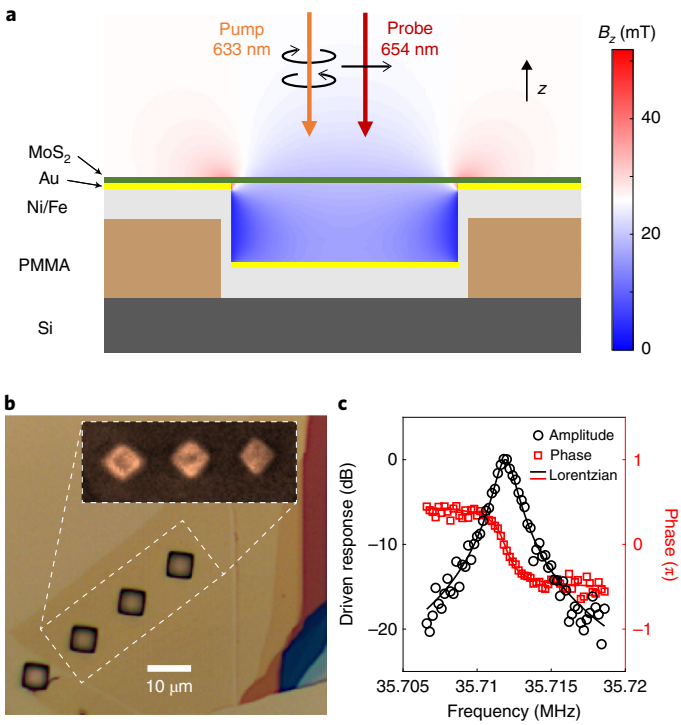

Fig. 2 | Monolayer MoS_2 valley–mechanical device. a, Cross-sectional schematic of the device, which consists of a monolayer MoS_2 suspended over square hole structures conformally coated with Ni/Fe permalloy films. Under an applied magnetic field, the permalloy structure induces a field gradient by distorting the local field. A pump laser (633 nm) whose polarizations are modulated between LCP and RCP is normally incident on the monolayer. The mechanical displacement is detected by a linearly polarized probe laser (654 nm) through interference between the lights reflected from the monolayer and the bottom gold surface (see Supplementary Information). The colour scale represents the magnitude of the z component of the magnetic field B_z simulated by a finite-element method. PMMA, poly(methyl methacrylate). **b**, The three holes on the upper right of the optical image are covered with monolayer MoS_2. The inset shows the photoluminescence emission from the devices. **c**, The thermo-optical driven mechanical response at a substrate temperature of about 20 K.

material is freestanding (inset of Fig. 2b). The lateral dimension of the square hole is $5.2 \times 5.2\,\mu m^2$, which gives a resonator effective mass of $m_{eff} = 21$ fg (see Supplementary Information).

We applied an optical interferometric scheme[29] to detect the mechanical displacement of the resonator using a continuous-wave probe laser (654 nm). Displacement detection responsivity was calibrated by reflection spectrum measurement (see Supplementary Information). The mechanical resonance of the device was characterized using an intensity-modulated pump light (633 nm) which thermo-optically drives the monolayer into mechanical resonance[25]. When the sample substrate was cooled from room temperature to 20 K, the resonance frequency f_m rose from 17.2 MHz to 35.7 MHz and the quality factor showed a dramatic increase from 120 to 22,000 (Fig. 2c). The increase in mechanical frequency is mainly caused by tensile stress building up at low temperature[27]. Throughout the measurement, minimal laser powers (11 μW for pump and 4 μW for probe) were used to avoid excessive optical absorption heating, which makes the nano-resonator unstable. The central region of the monolayer is estimated to have heated up by about 10 K relative to the substrate (Supplementary Fig. 8).

We observed the mechanical vibration actuated by valley carriers at cryogenic temperature (Fig. 3a). We alternately populated the K and K′ valleys by modulating the polarization of the pump beam (633 nm) between left-circularly polarized and right-circularly polarized (LCP and RCP) while keeping the light intensity constant (Supplementary Figs. 11 and 12). This results in a time-varying force $F(\omega)$ that drives the resonator. The measured displacement of the resonator $z(\omega)$ exhibits a Lorentzian response that follows the previously characterized mechanical susceptibility $\chi(\omega)$ (see Supplementary Information). In contrast, a pump light with linear polarizations does not show the driving effect. In this case, both valleys are equally populated and therefore the net force is zero. As we switched the pump polarization to opposite helicity, the mechanical displacement displayed a π-phase difference (Fig. 3b), which confirms that the populations of different valleys exert opposite forces onto the material. An opposite magnetic field gradient also induced a π-phase shift of the displacement by switching the sign of the force (Fig. 3b). Under our experimental conditions, the valley depopulation process (between picoseconds and a few nanoseconds[10,30–32]) is much faster than the pump polarization modulation (about 30 ns in periodicity). As a result, the polarization modulation is followed by the valley population in an adiabatic manner. To single out the valley–mechanical actuation and eliminate the effects of other forces, such as the thermo-optical or optical radiation pressure, a double lock-in technique is adopted where both the pump laser polarization and magnetic field gradient direction are being modulated (see Supplementary Information). Therefore, only the demodulated signals that correspond to both modulations are measured. In the experiment, the polarization of the probe light is kept linear to cancel its influence on the net valley population.

Given that occupation of different valleys gives rise to opposite forces, we were able to transduce the valley excitation to the mechanical states of the MoS_2 monolayer. We resonantly drove the device with opposite valley occupation and examined the two quadratures of the mechanical motion (Fig. 3c). Using a measurement bandwidth of 1 kHz with 1,024 averages, we resolved two distinct mechanical states of opposite phases and similar amplitudes, with a confidence level approaching unity (see Supplementary Information). This experiment verifies that the

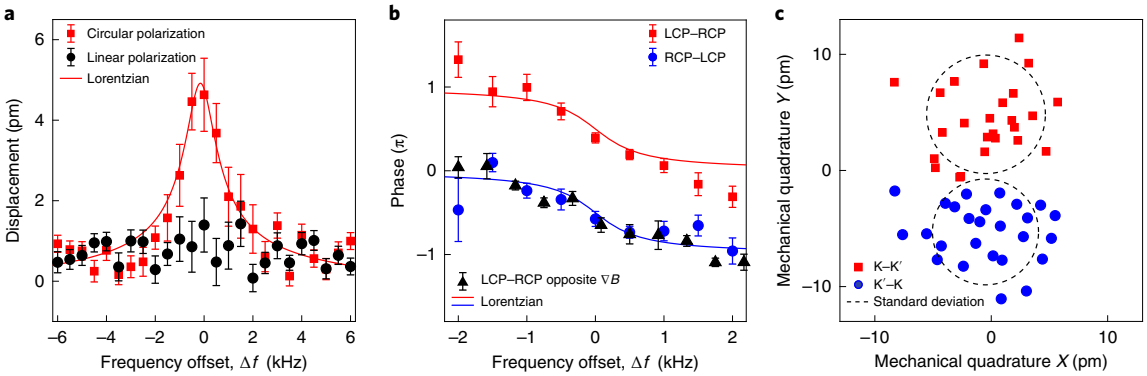

Fig. 3 | Experimental observation of valley-actuated mechanical motion. a, The driven displacement using the circularly polarized pump laser follows a Lorentzian trend, showing that the mechanical mode is excited by the valley–mechanical force. In contrast, the linearly polarized pump exhibits no driving signal as both valleys are populated equally. Δf is the frequency offset from the mechanical resonance. **b**, The phase response of the driven motion displays a π-phase difference when the polarization of the pump light is changed to opposite helicity or when the magnetic field gradient is switched to the opposite sign. **c**, The mechanical quadratures show two distinct states when the monolayer is driven resonantly by opposite valley excitation. The black dashed lines indicate the standard deviation of the datasets. The measurement is performed using a bandwidth of 1 kHz with 1,024 averages. In **a** and **b**, error bars are the standard errors of the signals and the sample temperature is about 30 K.

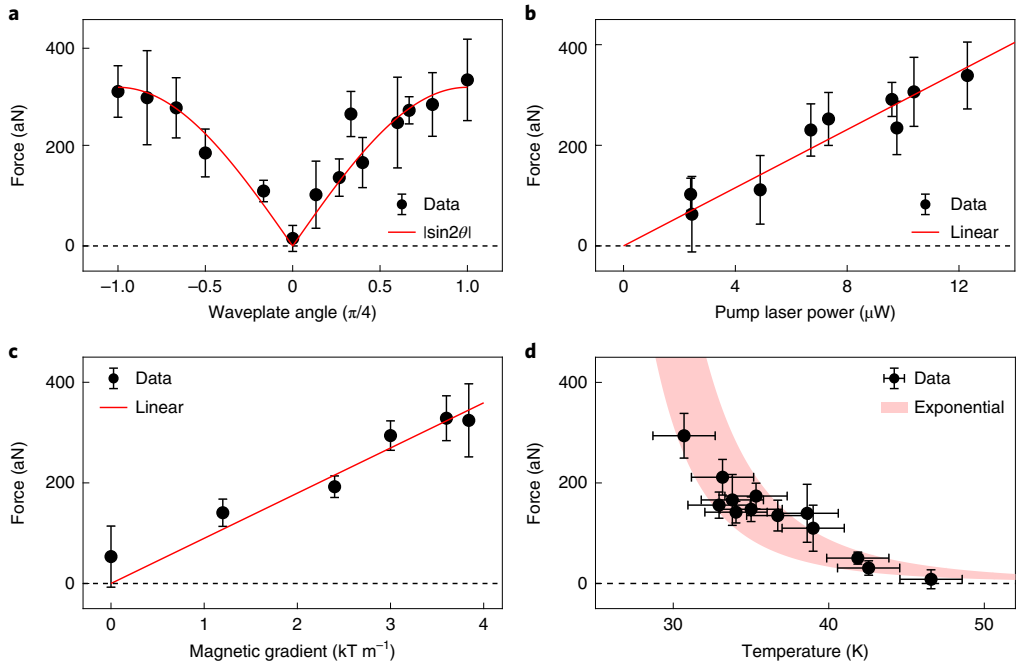

Fig. 4 | External control of the valley–mechanical force. a, The valley–mechanical force shows a $|\sin 2\theta|$ dependence (red line) as the angle θ between the quarter-wave plate axis and the pump laser polarization varies from $-\pi/4$ (LCP) to 0 (linearly polarized) to $+\pi/4$ (RCP). **b**,**c**, The valley–mechanical force shows a linear dependence (red lines) on the pump laser power and the magnetic field gradient. The field gradient is varied by changing the applied magnetic field perpendicular to the substrate and is calculated using the measured permeability of the permalloy film. **d**, The valley–mechanical force shows a strong dependence on temperature. The trend roughly follows $\exp(\Delta/k_B T)$ with $\Delta \approx 23$ meV. The red band represents the error estimates obtained from the fitting of the data with the exponential dependence. The laser heating effect is included to obtain the sample temperature (see Supplementary Information). In all panels, error bars represent the standard errors of the signals.

valley excitation can be directly transferred into mechanical states with negligible ambiguity.

We further quantifed the dependence of valley–mechanical force on the pump light and magnetic field gradient. We obtained the force through the measurement of the mechanical displacement and susceptibility. We varied the angle θ between the quarter-waveplate axis and the pump laser polarization from $-\pi/4$ (LCP) to 0 (linearly polarized) and to $+\pi/4$ (RCP), and found that the measured force had a $|\sin 2\theta|$ dependence (Fig. 4a), which verifies that the force is proportional to the net valley population ($N_K - N_{K'}$). This relation was further confirmed by a measurement of the pump power dependence (Fig. 4b). We also observed that the valley–mechanical force increases linearly as a function of the out-of-plane magnetic field gradient (Fig. 4c). This observation verifies

that the measured force is originated from the magnetic moment of the valley polarized carriers. The above findings demonstrate effective control over the valley–mechanical interaction through external conditions.

The valley–mechanical force also displays a strong dependence on temperature (Fig. 4d). The force becomes observable when the sample temperature is lowered below 46 K and rises steadily as the temperature is further reduced. These can be attributed to the increase of the steady-state valley populations at lower temperatures owing to longer carrier lifetimes. The temperature dependence of the valley–mechanical force roughly follows $\exp(\Delta/k_BT)$ with $\Delta \approx 23$ meV. This characteristic energy matches the phonon energy of monolayer MoS_2 at the K point, which suggests that such an activation behavior may be caused by phonon-assisted intervalley scattering[9,33]. With the measured valley–mechanical force of about 300 aN, we estimate the number of imbalance valley carriers to be about 2,000 and the valley polarization lifetime to be about 0.4 ns (see Supplementary Information).

An important parameter with which to quantify the valley–mechanical interaction is the single-phonon coupling rate $g_0 = g\mu_B \nabla B x_{zpf}/\hbar$, which describes the valley frequency shift induced by the quantum zero-point motion of the mechanical resonator $x_{zpf} = \sqrt{\hbar/4\pi f_m m_{\mathrm{eff}}}$. Benefiting from the large zero-point motion (0.11 pm) of the atomic thin resonator, $g_0/2\pi$ reaches 24 Hz in our experiment. The valley–mechanical coupling can be greatly enhanced by applying a stronger magnetic field gradient using magnetic nanostructures (up to $\nabla B \approx 10^7\,\mathrm{T\,m^{-1}}$)[34]. With the enhanced coupling, it is possible to realize valley–mechanical detection down to the single valley-pseudospin level. Furthermore, by using WSe_2/MoS_2 heterostructures to separate electron and hole layers, the valley lifetime can be extended to around 1 μs (ref. [35]). With these improvements, a single-valley cooperativity exceeding 1 is achievable (see Supplementary Information), which opens up possibilities for exploring the quantum coherent effects of valley–mechanical interaction.

We have realized the coupling between valley and mechanical degrees of freedom in a monolayer MoS_2 and demonstrated direct transduction of valley excitation into mechanical states. Our experiment suggests ways of realizing valley-actuated devices. One interesting example is the 'valley switch', which uses a valley signal to switch another valley signal—an analogue of the electronic transistor. This is possible by enhancing the valley–mechanical interaction to such a level that the mechanical backaction on the valley carriers becomes prominent (see Supplementary Information). Utilizing the mechanical element as an interconnect, such valley–mechanical coupling can also be implemented to hybridize valley pseudospin with microwave photons and superconducting qubits.

Online content

Any methods, additional references, Nature Research reporting summaries, source data, statements of code and data availability and associated accession codes are available at https://doi.org/10.1038/s41566-019-0428-0.

Received: 3 September 2018; Accepted: 29 March 2019;
Published online: 20 May 2019

References

1. Craighead, H. G. Nanoelectromechanical systems. *Science* **290**, 1532–1535 (2000).
2. Roukes, M. Nanoelectromechanical systems face the future. *Phys. World* **14**, 25–31 (2001).
3. Midolo, L., Schliesser, A. & Fiore, A. Nano-opto-electro-mechanical systems. *Nat. Nanotechnol.* **13**, 11–18 (2018).
4. Rycerz, A., Tworzydlo, J. & Beenakker, C. W. J. Valley filter and valley valve in graphene. *Nat. Phys.* **3**, 172–175 (2007).
5. Culcer, D., Saraiva, A. L., Koiller, B., Hu, X. & Sarma, S. D. Valley-based noise-resistant quantum computation using Si quantum dots. *Phys. Rev. Lett.* **108**, 126804 (2012).
6. Xu, X., Yao, W., Xiao, D. & Heinz, T. F. Spin and pseudospins in layered transition metal dichalcogenides. *Nat. Phys.* **10**, 343–350 (2014).
7. Mak, K. F., Xiao, D. & Shan, J. Light–valley interactions in 2D semiconductors. *Nat. Photon.* **12**, 451–460 (2018).
8. Xiao, D., Liu, G.-B., Feng, W., Xu, X. & Yao, W. Coupled spin and valley physics in monolayers of MoS_2 and other group-VI dichalcogenides. *Phys. Rev. Lett.* **108**, 196802 (2012).
9. Zeng, H., Dai, J., Yao, W., Xiao, D. & Cui, X. Valley polarization in MoS_2 monolayers by optical pumping. *Nat. Nanotechnol.* **7**, 490–493 (2012).
10. Mak, K. F., He, K., Shan, J. & Heinz, T. F. Control of valley polarization in monolayer MoS_2 by optical helicity. *Nat. Nanotechnol.* **7**, 494–498 (2012).
11. Mak, K. F., McGill, K. L., Park, J. & McEuen, P. L. The valley Hall effect in MoS_2 transistors. *Science* **344**, 1489–1492 (2014).
12. Ye, Z., Sun, D. & Heinz, T. F. Optical manipulation of valley pseudospin. *Nat. Phys.* **13**, 26–29 (2017).
13. Aivazian, G. et al. Magnetic control of valley pseudospin in monolayer WSe_2. *Nat. Phys.* **11**, 148–152 (2015).
14. Srivastava, A. et al. Valley Zeeman effect in elementary optical excitations of monolayer WSe_2. *Nat. Phys.* **11**, 141–147 (2015).
15. Ye, Y. et al. Electrical generation and control of the valley carriers in a monolayer transition metal dichalcogenide. *Nat. Nanotechnol.* **11**, 598–602 (2016).
16. Lee, J., Wang, Z., Xie, H., Mak, K. F. & Shan, J. Valley magnetoelectricity in single-layer MoS_2. *Nat. Mater.* **16**, 887–891 (2017).
17. Gubbi, J., Buyya, R., Marusic, S. & Palaniswami, M. Internet of Things (IoT): a vision, architectural elements, and future directions. *Future Gener. Comput. Syst.* **29**, 1645–1660 (2013).
18. Rebeiz, G. M. *RF MEMS: Theory, Design, and Technology* (John Wiley and Sons, 2004).
19. Kovacs, G. T. A. *Micromachined Transducers Sourcebook* (WCB/McGraw-Hill, 1998).
20. O'Connell, A. D. et al. Quantum ground state and single-phonon control of a mechanical resonator. *Nature* **464**, 697–703 (2010).
21. Palomaki, T. A., Harlow, J. W., Teufel, J. D., Simmonds, R. W. & Lehnert, K. W. Coherent state transfer between itinerant microwave fields and a mechanical oscillator. *Nature* **495**, 210–214 (2013).
22. Chu, Y. et al. Quantum acoustics with superconducting qubits. *Science* **358**, 199–202 (2017).
23. Bunch, J. S. et al. Electromechanical resonators from graphene sheets. *Science* **315**, 490–493 (2007).
24. Chen, C. et al. Performance of monolayer graphene nanomechanical resonators with electrical readout. *Nat. Nanotechnol.* **4**, 861–867 (2009).
25. Castellanos-Gomez, A. et al. Single-layer MoS_2 mechanical resonators. *Adv. Mater.* **25**, 6719–6723 (2013).
26. Lee, C., Wei, X., Kysar, J. W. & Hone, J. Measurement of the elastic properties and intrinsic strength of monolayer graphene. *Science* **321**, 385–388 (2008).
27. Morell, N. et al. High quality factor mechanical resonators based on WSe_2 monolayers. *Nano Lett.* **16**, 5102–5108 (2016).
28. Jensen, K., Kim, K. & Zettl, A. An atomic-resolution nanomechanical mass sensor. *Nat. Nanotechnol.* **3**, 533–537 (2008).
29. Wang, Z. & Feng, P. X.-L. Interferometric motion detection in atomic layer 2D nanostructures: visualizing signal transduction efficiency and optimization pathways. *Sci. Rep.* **6**, 28923 (2016).
30. Lagarde, D. et al. Carrier and polarization dynamics in monolayer MoS_2. *Phys. Rev. Lett.* **112**, 047401 (2014).
31. Yang, L. et al. Long-lived nanosecond spin relaxation and spin coherence of electrons in monolayer MoS_2 and WS_2. *Nat. Phys.* **11**, 830–834 (2015).
32. Plechinger, G. et al. Valley dynamics of excitons in monolayer dichalcogenides. *Phys. Status Solidi RRL* **11**, 1700131 (2017).
33. Carvalho, B. R. et al. Intervalley scattering by acoustic phonons in two-dimensional MoS_2 revealed by double-resonance Raman spectroscopy. *Nat. Commun.* **8**, 14670 (2017).
34. Tao, Y., Eichler, A., Holzherr, T. & Degen, C. L. Ultrasensitive mechanical detection of magnetic moment using a commercial disk drive write head. *Nat. Commun.* **7**, 12714 (2016).
35. Kim, J. et al. Observation of ultralong valley lifetime in WSe_2/MoS_2 heterostructures. *Sci. Adv.* **3**, e1700518 (2017).

Acknowledgements

We acknowledge support from the US Department of Energy, Office of Science, Office of Basic Energy Sciences, Materials Sciences and Engineering Division under contract number DEAC02-05-CH11231 (van der Waals Heterostructures Program, KCWF16) for theory, device fabrication and data analysis; from the King Abdullah University of Science and Technology (KAUST), Office of Sponsored Research (OSR) under award number OSR-2016-CRG5-2996 for sample preparation; and from the Office of Naval Research (ONR) MURI programme under grant number N00014-13-1-0631 for mechanical design and measurements.

Author contributions

K.Y.F., H.Z., H.-K.L. and X.Z. conceived the project. H.-K.L. and K.Y.F. designed the experiment and performed the measurement. K.Y.F., H.-K.L., S.W. and S.Y. fabricated the substrate. H.-K.L., Q.L. and S.W. performed the MoS_2 transfer. H.-K.L., K.Y.F., H.Z. and X.Z. analysed the data and wrote the manuscript with inputs from all authors. X.Z., Y.W. and S.Y. guided the research.

Competing interests

The authors declare no competing interests.

Additional information

Supplementary information is available for this paper at https://doi.org/10.1038/s41566-019-0428-0.

Correspondence and requests for materials should be addressed to X.Z.

Methods

Methods relating to sample fabrication, characterization of the materials, measurement set-up, signal acquisition and data analysis (and associated references) are available in the Supplementary Information. After the submission of this manuscript, the technical part was presented at a conference[36].

Data availability

The data that support the plots within this paper and other findings of this study are available from the corresponding author upon reasonable request.

References

36. Fong, K. Y. et al. Valley-optomechanics in a monolayer semiconductor. *Proc. SPIE* **10733**, 107330E (2018).